Cochlear implants: Modeling electrophysiological responses

Gendt, M.J. van

Citation

Gendt, M. J. van. (2021, March 25). *Cochlear implants: Modeling electrophysiological responses*. Retrieved from https://hdl.handle.net/1887/3149359

Note: To cite this publication please use the final published version (if applicable).

Cover Page

The handle http://hdl.handle.net/1887/3149359 holds various files of this Leiden University dissertation.

Author: Gendt, M.J. van
Title: Cochlear implants: Modeling electrophysiological responses
Issue date: 2021-03-25

CHAPTER 2

A fast, stochastic, and adaptive model of auditory nerve responses to cochlear implant stimulation

Margriet J. van Gendt

Jeroen J. Briaire

Randy K. Kalkman

Johan H.M. Frijns

Abstract

Cochlear implants (CIs) rehabilitate hearing impairment through direct electrical stimulation of the auditory nerve. New stimulation strategies can be evaluated using computational models. In this study, a computationally efficient model that accurately predicts auditory nerve responses to CI pulse train input was developed. A three-dimensional volume conduction and active nerve model developed at Leiden University Medical Center was extended with stochasticity, adaptation, and accommodation. This complete model includes spatial and temporal characteristics of both the cochlea and the auditory nerve. The model was validated by comparison with experimentally measured single fiber action potential responses to pulse trains published in the literature. The effects of pulse rate and pulse amplitude on spiking patterns were investigated. The modeled neural responses to CI stimulation were very similar to the single fiber action potential measurements in animal experiments. The model's responses to pulse train stimulation with respect to spatial location were also investigated. Adaptation was stronger at the borders of the stimulated area than in the center. By combining spatial details with long-term temporal components and a broad implementation of stochasticity a comprehensive model was developed that was validated for long duration electric stimulation of a wide range of pulse rates and amplitudes. The model can be used to evaluate auditory nerve responses to cochlear implant sound coding strategies.

1 Introduction

Cochlear implants (CIs) are implantable devices that partially restore auditory perception in individuals who have severe to profound hearing loss. CIs generally provide good speech understanding in quiet and have become the established mode of rehabilitation for adults with severe to profound hearing loss (Clark and Clark, 2013). However, CI users still experience difficulties understanding speech in noisy (real life) situations and suboptimal encoding of pitch accents due to limited transfer of the fine spectrotemporal details of the sound (Wouters et al., 2015). Many different sound-coding strategies have been introduced in the last decade to overcome this challenge, but no major advances have been made since the introduction of the Continuous Interleaved Sampling (CIS) strategy (Wilson et al., 1991; Zeng et al., 2008). New stimulation strategies are commonly investigated in psychophysical experiments and clinical trials, which is time-consuming for both the patient and researcher. Alternatively, strategies can be evaluated with the use of computational models. The present study presents a computationally efficient model that accurately predicts auditory nerve responses to arbitrary CI input signals.

A comprehensive computational model of the response of the auditory nerve to CI stimulation should include a realistic distribution of thresholds of all nerve fibers, and take into account both stochastic behavior and history effects. Stochasticity generally plays a role in the human sensory system (Verveen and Derksen, 1968) and is present in the auditory nerve's responses to electrical stimulation (Rubinstein, 1995). Animal experiments have demonstrated variance in neural responses to different pulses in a pulse train (Bruce et al., 1999a, 1999b; Dynes and Delgutte, 1992; Miller et al., 1999a; Shepherd and Javel, 1997). In addition, animal experiments (Cartee et al., 2000; Litvak et al., 2001; Miller et al., 2008; Zhang et al., 2007) have shown a dependency of auditory nerve behavior on previous neural spikes and pulses, referred to as the history effects. Here, history effects include refractoriness, facilitation, adaptation, and accommodation. Refractoriness is the diminished excitability of the nerve immediately following an action potential. Facilitation is a threshold decrease caused by a preceding sub-threshold pulse. Adaptation refers to a threshold increase caused by long-term firing of the neuron. Accommodation refers to a threshold increase caused by a long-term stimulation current and occurs when the membrane slowly depolarizes due to the stimulus. Accommodation and adaptation recently received increased attention as important aspects in neural responses to long duration electrical stimulation (Hay-McCutcheon et al., 2005; Hughes et al., 2012; Liu and Wang, 2001; Negm and Bruce, 2014, 2008; Woo et al., 2010, 2009). Neural adaptation, a decrease in neural excitability during persistent stimulation, is important for efficient coding of dynamically varying inputs (Bohte, 2012; Drew and Abbott, 2006; Zilany and Carney, 2010). Although some early research was equivocal about the existence of auditory nerve adaptation in response to electrical stimulation (Parkins, 1989), several reports indicate that electrical stimulation leads to adaptation of the auditory nerve (Javel et al., 1987; van den Honert and Stypulkowski, 1987). Several groups have investigated the effects of long duration continuous or pulsatile electrical stimulation on nerve activation

based on single fiber action potential (SFAP) measurements of the auditory nerve (Dynes and Delgutte, 1992; Hartmann et al., 1984; Javel et al., 1987; Shepherd and Javel, 1997; van den Honert and Stypulkowski, 1987). In order to predict the performance of patients with CIs in discrimination tasks, the complete nerve fiber's response has to be predicted. A complete cochlear model is required to investigate the responses of the auditory nerve in both the spatial and temporal domain. A model of the whole nerve is needed to investigate the influence of the spatial location of auditory nerve fibers on temporal response patterns.

Different types of models are available to predict nerve responses to electrical stimulation. A major distinction can be made between the biophysical and phenomenological type of models. Biophysical models quantitatively describe nerve membrane behavior in response to an induced membrane current and have been shown to correctly predict membrane responses to single pulses and reasonably predict latencies, refraction, and facilitation effects (Frijns et al., 1994; Frijns and ten Kate, 1994; Reilly et al., 1985; Schwarz and Eikhof, 1987). These models can be combined with 3D volume conduction models of the cochlea to predict auditory nerve responses to electrical pulses as reported by Kalkman et al. (2015). Biophysical model parameters are based on patch-clamp single fiber recordings, from which high order effects, required to model responses to long duration pulse trains, are difficult to obtain. In addition, the calculation of responses to long duration pulse trains using these models requires long computational times. Phenomenological models directly relate empirical observations to expected neural output. Such models have been used to efficiently predict responses to sustained stimulation by direct implementation of stochastic and temporal behavior (Bruce et al., 1999a, 1999b; Chen and Zhang, 2007; Litvak et al., 2003a; Macherey et al., 2007; Stocks et al., 2002; Xu and Collins, 2007). All proposed phenomenological approaches modeled auditory nerve fibers as single nodes and incorporated at most 20,000 fibers. The models that included a geometric current spread all modeled the electrode contacts as point sources located in homogeneous media. Phenomenological models that simulate thresholds are only capable of dealing with pre-defined pulse shapes.

The goal of the current study was to develop a hybrid model that incorporates spatial and pulse-shape effects from a biophysical model, as well as temporal effects and stochastic responses from a phenomenological model. The model had to be computationally efficient in order to predict whole nerve responses to long duration pulse trains. By merging the biophysical and phenomenological approaches in a compound model, we utilized the merits of both methods and minimized their disadvantages. The model was validated by comparison with experimentally measured SFAP responses to pulse trains published in the literature. The model's output with regards to discharge rate, rate variances, rate decreases, and pulse intervals was evaluated for pulse trains with different rates and amplitudes. For clarity the comparison between model predictions and animal data from the literature will be given directly in the results section. In the discussion section the

similarities and differences between predictions and data will be interpreted and analyzed in terms of model parameters.

2 Materials and methods

2.1 Model

The model presented in this paper builds on the previously published 3D volume conduction model of the cochlea and deterministic cable model of the human auditory nerve (Kalkman et al., 2015). The cochlear geometry is based on micro-CT data, the electrode array geometry is based on the HiFocus1J, modelled in lateral position. The model presented in this paper extends the deterministic thresholds from active GSEF nerve fibers (Briaire and Frijns, 2005; Frijns et al., 2000) with stochastic behavior and history effects (Figure 2.1). Deterministic thresholds are obtained at 3200 spatially different locations using the 3D volume conduction model, an overview of the model is shown in Figure 2.2; for details of its implementation we refer to Kalkman et al. (2015). At each of these locations, 10 different nerve fibers are modeled. Thus, the model of the whole auditory nerve effectively incorporates a total of 32,000 different auditory nerve fibers. The deterministic thresholds of the 3D model are used as input to the phenomenological model extension; only the thresholds of entire fibers are taken into account, and not the individual thresholds of each Ranvier node. For each nerve fiber, stochasticity is induced by adding a relative spread (RS) to the deterministic thresholds. To account for refractoriness these stochastic thresholds are elevated depending on the time since the last spike relative to refractory period. Spike adaptation (SA) and accommodation are included by increasing the threshold after each spike and pulse.
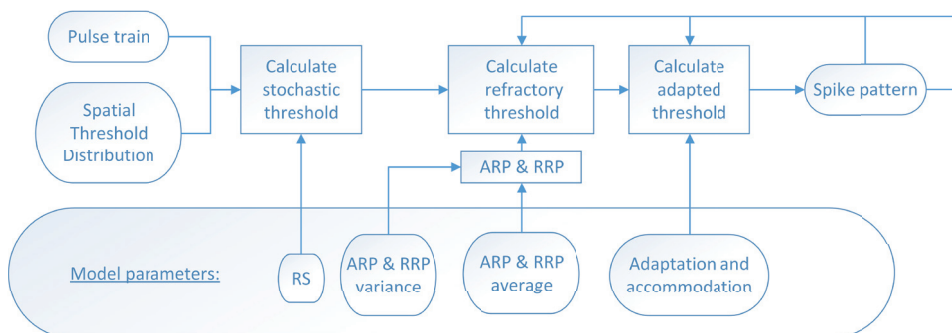

Figure 2.1. Model flow-chart per fiber. The deterministic threshold is input to the model that includes a relative spread, refractoriness, adaptation and accommodation. The final calculated thresholds are compared to the stimulus input to predict whether or not an action potential has occurred.
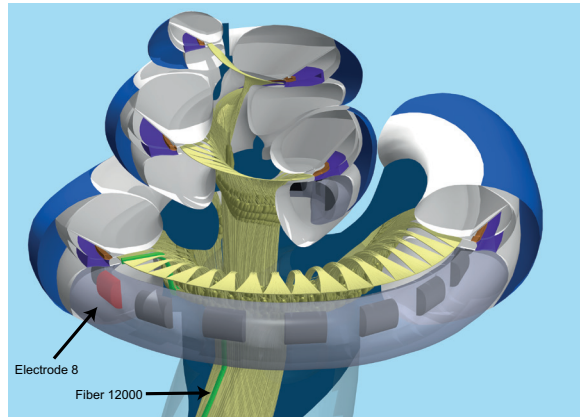
Figure 2.2. 3D model overview. Unless stated otherwise, the simulations were done by stimulating the electrode located at roughly 175 degrees from the round window, here highlighted in red. Most of the simulations were done on fiber 12000 (fiber 1200 in the 3D model), here highlighted in green; fibers are counted from basal to apical cochlear locations. The tip of this fiber is located roughly at the same cochlear angle as the stimulated electrode.

In order to develop a model that predicts neural responses to situations different than the ones exactly replicated during the validation, model parameters were based on physiological data. For every parameter the values and references are described below. A distinction can be made between parameters for which the values could be drawn directly from the literature (refractoriness, stochasticity and the adaptation time constant) and parameters which were based on fits to experimental data (adaptation and accommodation amplitudes). Because of this approach the model predictions are generalizable to other experiments than the ones presented in this paper. The mean and variance of the model parameters RS, absolute refractory period (ARP), and relative refractory period (RRP) are based on the literature. For each fiber, a specific value is drawn from these normal distributions. For the simulations in this paper, monopolar stimulation with cathodic-first biphasic pulses and a pulse width of 18 µs was used and is the stimulus was strong enough an action potential was assumed to occur during the anodic phase. The model uses time steps in the size of the pulse width; in other words, in the presented simulations every 18 µs the model calculates which fibers are expected to fire. The extended temporal and stochastic model was developed in Matlab (Mathworks, Inc.). The configuration of stimulation and measurement in the model is shown in figure 2.2. The electrode contact coloured red is the stimulating contact in the simulations presented in the paper. Most of the recordings are done on a fiber at the location coloured green. In the simulations the action potential is recorded at the end of the fiber to exclude effects of aborted spikes (Frijns et al., 1994). Typical inputs and outputs to this extension of the complete model are shown in figure 2.3. Figure 2.3A shows the typical stimulation waveform, where in the presented simulations the Phase Duration (PD) was set to 18 µs and amplitudes were variable. Figure 2.3B shows an example neural excitation threshold

distribution as obtained using the 3D volume conduction and active nerve fiber model. Figure 2.3C and 2.3D show an example spike pattern and its corresponding Post Stimulus Time Histogram. This example is obtained by measuring the response at fiber 12000.
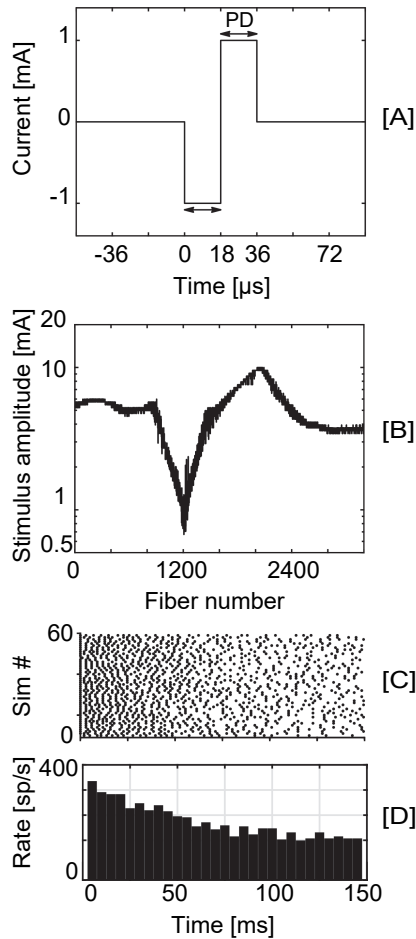
2

Figure 2.3. Model input and output. An example of the stimulating waveform used in the current simulations is shown in [A]. The deterministic threshold of all fibers was calculated using the 3D model and the active nerve model. An example of the threshold waveform, in the spatial dimension, in response to stimulation of one electrode is shown in [B]. The output of the model is a spiking pattern. An example of spike patterns in 50 different trials to an identical stimulus (1000 pps, 150 ms, amplitude 0.85 mA) is shown in [C] and its corresponding Post Stimulus Time Histogram in [D].

Relative spread of thresholds

A measure of the variability of spike initiation is the RS, which is defined as the standard deviation (SD) of the underlying Gaussian distribution divided by its mean (Verveen and Derksen, 1968). The SD of the normal distribution around the deterministic threshold is defined as: SD = Idet · RS, where Idet is the deterministic single pulse threshold for an individual fiber. Idet is the minimal current required on the selected electrode to elicit an action potential in the fiber that is strong enough to run all the way to the end of the modelled axon, regardless of the node at which the fiber was excited initially. Idet was calculated using the 3D volume conduction and the deterministic nerve model. Using the RS, the spiking probability can be calculated using a phenomenological approach, similar to Bruce et al. (1999b). After each pulse, the stochastic threshold is obtained from the normal distribution, N(Idet,SD). The RS, an estimate of the stochastic behavior of the auditory nerve, is obtained from measurements of the SFAP (Bruce et al., 1999b; Javel et al., 1987; Miller et al., 1999a). An overview of RS values described in the literature is given in table 2.1. In the model, the RS is set to 0.06 with a SD of 0.04 and a minimum of 0, within the range of the various distributions found in the literature for comparable pulse widths.

Table 2.1. Relative Spread (RS) estimates obtained from SFAP measurements published in literature, PD = Phase Duration, RS = Relative Spread, SD = Standard Deviation

Author (year)	Stimulus	RS (SD)
Bruce et al. (1999b) from Javel et al (1987)	PD 200 us, biphasic	0.12 (0.05)
	PD 400 us, biphasic	0.11 (0.04)
Bruce et al. (1999b) from Dynes (1996)	PD 100-200 us, cathodic	0.12 (0.06)
Miller et al. (1999)	PD = 26 us, cathodic	0.06 (0.03)
	PD = 26 us, anodic	0.06 (0.04)
	PD = 39 us, cathodic	0.06 (0.04)
	PD = 39 us, anodic	0.07 (0.07)

Refractoriness

The ARP is the period immediately following an action potential during which the neural membrane is unable to fire again. The ARP is followed by the RRP, during which only a greater than normal stimulus can induce a response. Refractoriness can be implemented as a threshold increase following an action potential. The refractoriness factor, R, is calculated using equation 2.1:

$$R = \frac{1}{1 - e^{\frac{-(t-\tau_{ARP})}{\tau_{RRP}}}}$$
(Eq. 2.1)

where τARP and τRRP are the time constants for the ARP and RRP, and t is the time since the last action potential. Equation 2.4 below shows how R is used to calculate the final threshold. Estimates for the ARP and RRP of the auditory nerve can be obtained directly using the SFAP (Dynes, 1996; Miller et al., 2001, 1999a), extracted from model data (Bruce et al., 1999a) or estimated based on human electrically evoked Compound Action Potential (ECAP) measurements (Cartee et al., 2000; Stypulkowski and Van den Honert,

1984). Figures 2.4A and 2.4B show the estimates for τARP and τRRP, respectively. The average values and SDs for τARP and τRRP were chosen so they closely mimic the range of values found in the literature (figure 2.4). τARP is set to 0.4 ms (SD 0.1 ms) and τRRP to 0.8 ms (SD 0.5 ms). For each of the 32,000 modeled fibers, values for τARP and τRRP were randomly chosen from the normal distribution. Additional randomness is applied to the refractoriness by choosing the final ARP and RRP at every time point from a distribution with a SD of 5% of the average (Hamacher, 2004). If the value obtained for one of the refractory parameters is less than zero, its value is set to zero.
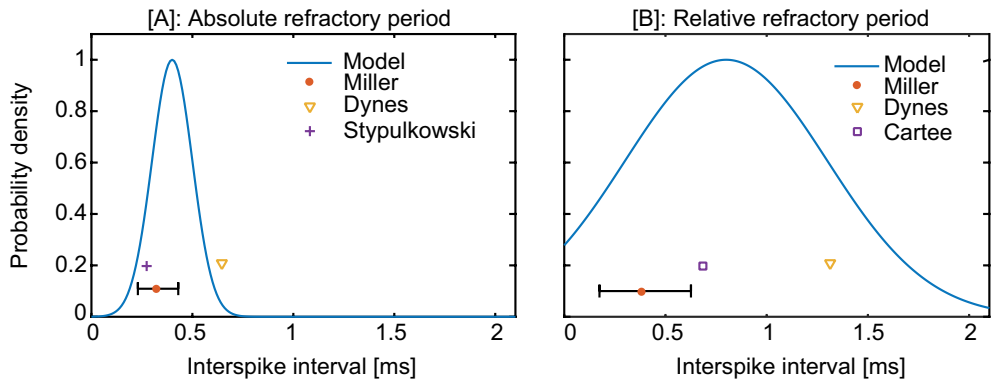

Figure 2.4. Absolute [A] and relative [B] refractory periods. The blue lines indicate the distribution of both model parameters as used in the proposed model. The other symbols indicate values published in the literature for both model parameters. If a standard deviation was also reported this is included as an error bar.

Spike adaptation and accommodation

The model extension described in this paper includes both firing-dependent adaptation and stimulus-dependent adaptation, with the latter referred to as accommodation. As first described by Litvak et al. (2001), auditory nerve responses exhibit larger adaptation in response to higher rate pulse trains. In order to obtain a stronger reduction in spike rates with higher stimulus rates, regardless of the initial discharge rate, an adapting parameter had to be introduced into the model that depends on pulse history, not on spiking history. To account for this effect, the accommodation parameter is included. The fiber adapts after each spike and accommodates after each pulse given. The spike adaptation (SA) is calculated as in equation 2.2, where i are all previous spikes, t is the current time, and t_i is the time since spike i.

$$SA = \sum_i ampl_{adap} \cdot e^{\frac{t - t_i}{\tau_{adap}}}$$

(Eq. 2.2)

The adaptation amplitude is taken from a normal distribution with an average of 1.0% of the threshold and a SD of 0.6% of the threshold.

The accommodation (acco) is calculated as in equation 2.3, where p are all previous pulses, t is the current time, and tp is the time since pulse p.

$$Acco = \sum_p 0.03\% \cdot I \cdot \frac{I_{\min}(electrode)}{I(electrode, fiber)} \cdot e^{\frac{t-t_p}{\tau_{adap}}}$$ (Eq. 2.3)

The accommodation parameter is modeled as a threshold increase after each pulse as large as 0.03% of the given stimulus current multiplied by a spatial factor. The spatial factor for each fiber and electrode is the minimum current required to elicit a spike on any of the fibers using the concerned electrode, divided by the current required to elicit a spike in the simulated fiber with this electrode: $\frac{I_{\min}(electrode)}{I(electrode, fiber)}$. Thus, the accommodation is strongest at the fibers with the lowest thresholds. Both the accommodation and the adaptation parameter are forced to have a positive value for every fiber.

Dynes and Delgutte (1992) suggested that adaptation to electric sinusoids follows a single negative exponential course across several hundreds of milliseconds. More recently, several research groups studied the adaptation of responses to high-rate biphasic electrical stimulation with CIs (Litvak et al., 2001; Miller et al., 2008; Zhang et al., 2007). Litvak et al. (2001) found a short-term (< 150 ms) adaptation that is dependent on pulse rate. Investigating spike rates for pulse trains up to 5000 Hz, Zhang et al. (2007) and Miller et al. (2008) found asymptotic values within 300 ms of stimulation. The amount of adaptation was affected by pulse rates and stimulus levels and fit to an exponential decaying model with two different time constants: a rapid adaptation of 10 ms and a short-term adaptation of 100 ms. In the current model, both spike adaptation and accommodation are modeled as decaying exponentially with a time constant of 100 ms.

Final threshold
For every fiber, the final adjusted threshold (Iadj) is calculated as in equation 2.4.

$$I_{adj} = N(I_{det}, \sigma) \cdot R + SA + Acco$$ (Eq. 2.4)

A spike is assumed to occur if: $I_{given} > I_{adj}$, where I_{given} is the stimulus current. The overall parameter set used in the model is given in table 2.2.

Table 2.2. Overall parameter set as used in the model

Parameter	Value (± SD)
RS	0.06 (±0.04)
T_{ARP}	0.4 (±0.1) ms
T_{RRP}	0.8 (±0.5) ms
Within Refractoriness stochasticitiy	5% of τ_{ARP} / τ_{RRP}
Adaptation amplitude	1.0 (± 0.6)% of threshold
Accommodation amplitude	0.03% of pulse current · spatial factor

2.2 Validation

To validate the outcomes of the model, animal experiments published in the literature were emulated (Javel et al., 1987; Litvak et al., 2001; Miller et al., 2008; Zhang et al., 2007). The experiments were SFAP measurements performed in cats. Unless noted otherwise, the simulations were done by stimulating the electrode located at roughly 175 degrees from the round window. Most of the simulations were done on fiber 12000, fibers are counted from basal to apical cochlear locations. This fiber is located roughly at the same angle as electrode 8, close to its center of stimulation. Both electrode 8 and fiber 12000 (which corresponds to fiber 1200 in the 3D model) are highlighted in figure 2.2. Because of the multitude of different experiments, a variety of set-ups were investigated. In validation experiments that included a group of nerve fibers, the model parameters of the different fibers were randomly drawn from the distributions given in table 2.2. In some of the experimental data only the recordings of a single fiber are shown. The characteristics of the modeled fiber used to reproduce these data were always set to the average value presented in table 2.2. Except for the discharge rate I/O curves, which were calculated by simulating a nerve one time, all outcome measures were obtained by simulating one fiber several times. For the interval histograms (IHs), five averages were used; for all other simulations 30 averages were used.

The effect of stimulus amplitude on overall discharge rate was investigated by evaluating the discharge rate I/O curves using 100 ms pulse trains of different rates: 100, 200, 300, 400, 600, and 800 pulses per second (pps), in accordance with experiments done by Javel et al. (1987). Average discharge rates were calculated over the whole period of stimulation. For this simulation, the average model parameters were used. The animal experiments were previously simulated using a phenomenological model by Bruce et al (1999a). Their results also included normalized values for the first spike of the pulse train. Similar to the approach of Bruce et al, the model was used to predict these by turning off all inter-pulse effects. The variances in the responses are also presented in the paper by Bruce et al. and simulated using the proposed model for rates of 200 and 600 pps.

To emulate the data published by Zhang et al. (2007), post-stimulus time histograms (PSTHs) for a fiber in response to 300 ms pulse trains were modeled. Discharge rates during the complete stimulus, calculated as the number of spikes during small time segments, were plotted in PSTHs with binwidths of 1 ms. Stimulus pulse rates were 250, 1000, 5000, and 10,000 pulses/s. Amplitudes of 0.8, 0.9, and 1 mA were used. For this simulation, all model parameters were set to the average values.

In order to compare to data from Miller et al. (2008), the timing of spikes in response to 300 ms pulse trains at different rates and amplitudes was investigated using IHs, which plot timings between consecutive spikes in response to a pulse train. To investigate changes in inter-spike timings over the duration of the stimulus IHs were obtained for simulated responses to 300 ms pulse trains of 250, 1000, and 5000 pps at three different temporal epochs; 0-12 ms, 4-50 ms, and 200-300 ms.

To investigate how the model accounts for adaptation and accommodation, spike rate decrements in response to pulse trains with different rates were calculated. Group data on spike rate decrements were obtained to replicate the measurements of multiple fibers by Litvak et al. (2001). Discharge rate decrements were obtained by calculating the difference between the final and initial discharge rates in response to 1200 and 4800 pps pulse trains for a large number of fibers. The discharge rate decreases measured for a group of nerve fibers by Zhang et al. (2007) were also simulated. The spike rate decrements at four different stimulus pulse rates (250, 1000, 5000, and 10,000 pps) were calculated.

2.3 Whole nerve simulations

To see the effect of the 3D volume conduction model on discharge rates in the whole nerve, all 32.000 fibers were stimulated for a period of 200 ms. The average discharge rates of all fibers over the duration of the stimulus were compared to the deterministic single pulse thresholds obtained using the 3D volume conduction and active nerve fiber model. Whole nerve simulations were performed to investigate the total nerve activation and the effect of the spatial distribution of nerve fibers relative to the electrode on the temporal response. Simulations were performed with a loud (1.4 mA) continuous pulse train of 150 ms and 5000 pulses/s presented to the stimulating electrode. The temporal spiking pattern of fibers at different geometric locations was investigated.

3 Results

3.1 Spike rate growth I/O curves and variances

Simulated discharge rate I/O curves calculated for different rate pulse trains (figure 2.5A) mimicked animal experiments done by Javel et al. (1987) (figure 2.5B).

The discharge rate in response to the 800 pps pulse train in both simulations and experiments increased from 0 to 700 spikes/s when stimulus amplitude increased with 8 dB. The slopes for lower rate pulse trains were shallower in both the animal data and simulations, which was most clearly visible at 100 pps. To visualize this effect an I/O curve at these lowest rates is obtained for a fiber with all parameters set to average, shown in figure 2.6. As clearly visible in this figure, the rate increases most with amplitudes for higher stimulation rates. In both the animal data and simulations, the I/O curves exhibit a rocky increase in the discharge rate with increasing amplitude. Because the absolute amplitudes are dependent on the electrode configuration and placement, which is very different in the experimental set-up and modeled situation, only relative amplitude differences are relevant.
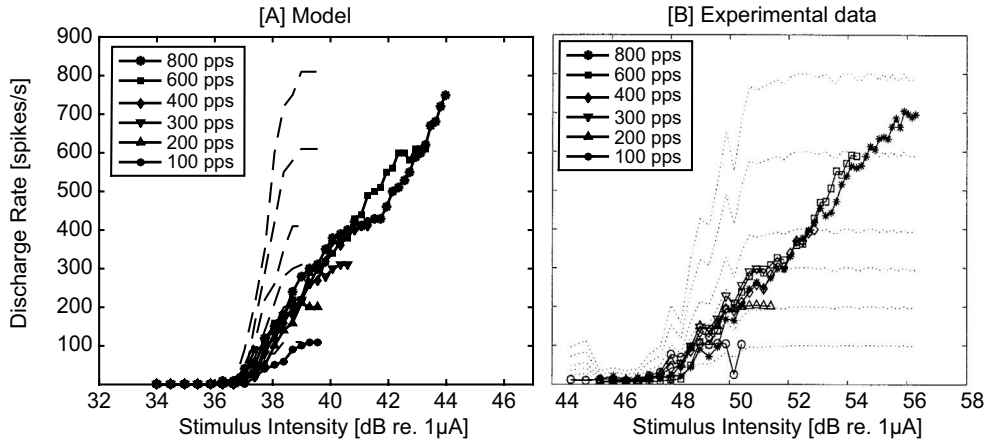
Figure 2.5. Mean discharge rates simulated with the current model [A] and results obtained with animal experiments [B] (Javel et al., 1987, reprinted with permission(1987)), at pulse rates of 100, 200, 300, 400, 600 and 800 pulses/s. Amplitudes used for the simulations ranged from 0.5 to 1.6 mA with a step size of 0.03 mA. Every data point was obtained from a single trial. Once the discharge rate equaled the stimulus rate only a few higher steps in amplitude were simulated, as was done in the animal experiments. Dotted lines indicate normalized values for the first spike of the pulse train. Similar to the approach of Bruce et al, the model was used to predict these by turning off all inter-pulse effects.

The variance measures shown by Bruce et al were also simulated with the proposed model, results are shown in figure 2.7. Larger variance per pulse is seen for the lower pulse rates, especially around 0.5 discharge probability per pulse. At this discharge probability per pulse the variance shows a dip, as is also seen in the animal data. Changing parameters for RS and the refractory periods gives different variability behavior. The refractoriness, as suggested by the authors of the paper of Bruce et al, as well as the RS, influences the shape of these curves.
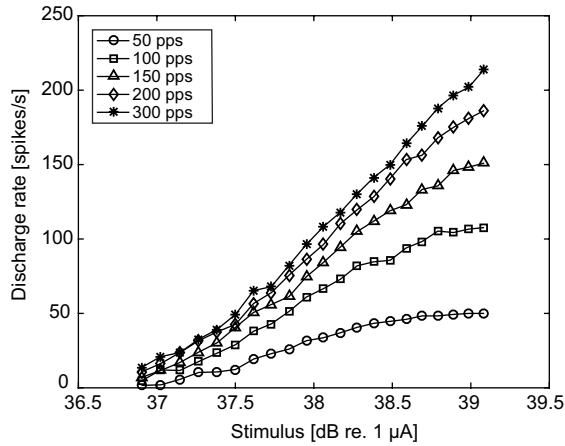
Figure 2.6. I/O-curves of discharge rate increases with increased stimulus amplitude for 5 different pulse rates: 50, 100, 150, 200 and 300 Hz. The x-axis plots the amplitude in dB relative to 1 μA, 30 trials were done.
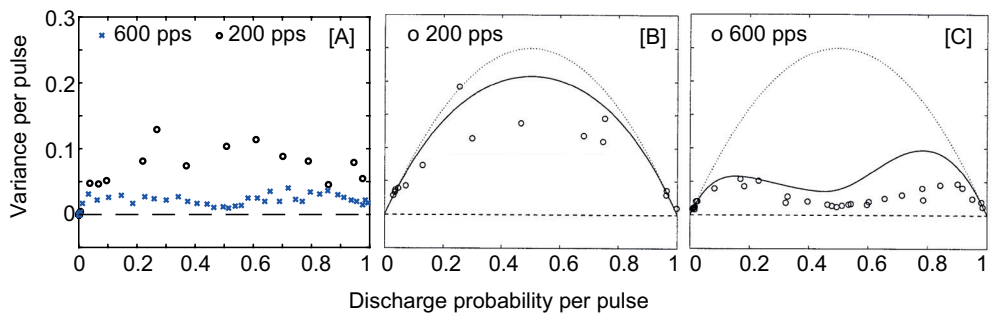

Figure 2.7. Variance per pulse versus discharge rate probability per pulse with the here presented model [A] and previous recordings and models [B and C] (Bruce et al., 1999, reprinted with permission). In [A] simulations are shown with 200 and 600 pps, all model parameters were set to average, amplitudes ranged from 0.5 to 1.5 with a step size of 0.01. In [B] (200 pps) and [C] (600 pps) the circles represent animal recordings, the lines represent previous models.

3.2 Post-stimulus time histograms

The PSTHs obtained using the model for two different fibers in response to a 300 ms pulse train for different pulse rates and amplitudes are shown in figure 2.8A. These histograms replicate data published by Zhang et al. (2007), which is shown in figure 2.8B.
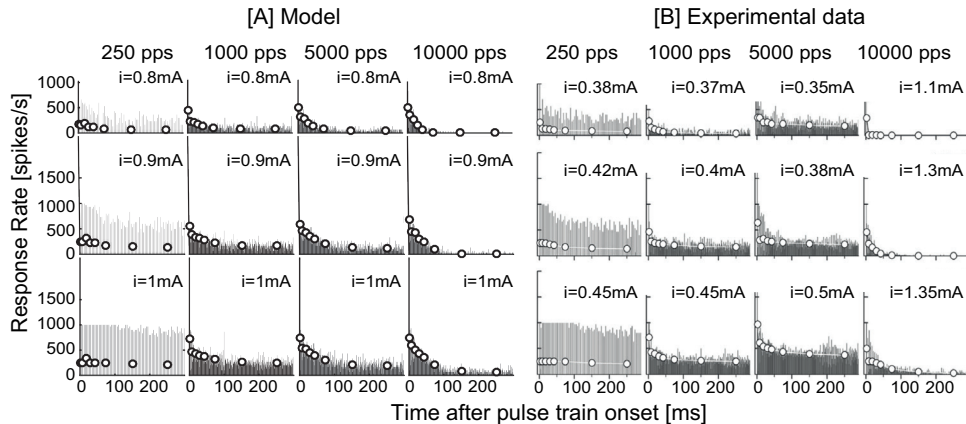
Figure 2.8. Post Stimulus Time Histograms. Examples of PSTHs obtained with simulations [A] and animal experiments [B] (Zhang et al., 2007, reprinted with permission) from the responses of an auditory nerve fiber (ANFs) at four different stimulus rates; 250, 1000, 5000 and 10.000 pps. Each column contains responses to stimulus trains of 3 different amplitudes. Amplitudes used for the simulations were 0.8, 0.9 and 1.0 mA. The vertical lines in the PSTH's are response rates during bins with a width of 1 ms. The open circles indicate the PSTH in binwidths with increasingly large bin-sizes: 0-4, 4-12, 12-24, 24-36, 36-48, 48-100, 100-200 and 200-300 ms.

All model parameters were set to the average values. When stimulated with the lowest pulse rate (250 pps, left column), the discharge rate in both the animal and simulation data decreased from around 800 pps initially to approximately 400 pps at the lowest amplitude, from 1000 pps to approximately 600 pps within the first 100 ms for the middle amplitude, and from 1000 to approximately 800 after 200 ms when stimulated with the highest amplitude. When stimulated with 1000 pulses/s, the discharge rates decrease much faster, within the first 50 ms for both animal experiments and simulations. The discharge rates in the animal and simulation data decreased from around 400 pps initially to approximately 100 pps at the lowest amplitude, from 500 pps to approximately 200 pps for the middle amplitude, and from 1000 to approximately 300 when stimulated with the highest amplitude. When stimulated with the 5000 pps pulse train, initial discharge rates were higher than when stimulated with the 1000 pps pulse train, and the decrease in discharge rate occurred later (around 50 ms) in both the animal data and simulations. However, the decrease in discharge rate was larger in the simulation than in the animal data. When stimulated with the highest rate pulse train (10, 000 pps) the strongest adaptation for all different amplitudes in both the simulations and animal experiments

were seen. In the animal experiments much larger stimulus amplitudes were used, and a different fiber was stimulated. The modeled fiber showed a smaller decrease in discharge rate at larger stimulus amplitudes. It was tested that by choosing a fiber with larger adaptation characteristics in the model, or a fiber more off-center of stimulation, a decrease in discharge rate similar to animal experiments is seen at these high amplitudes and rates.
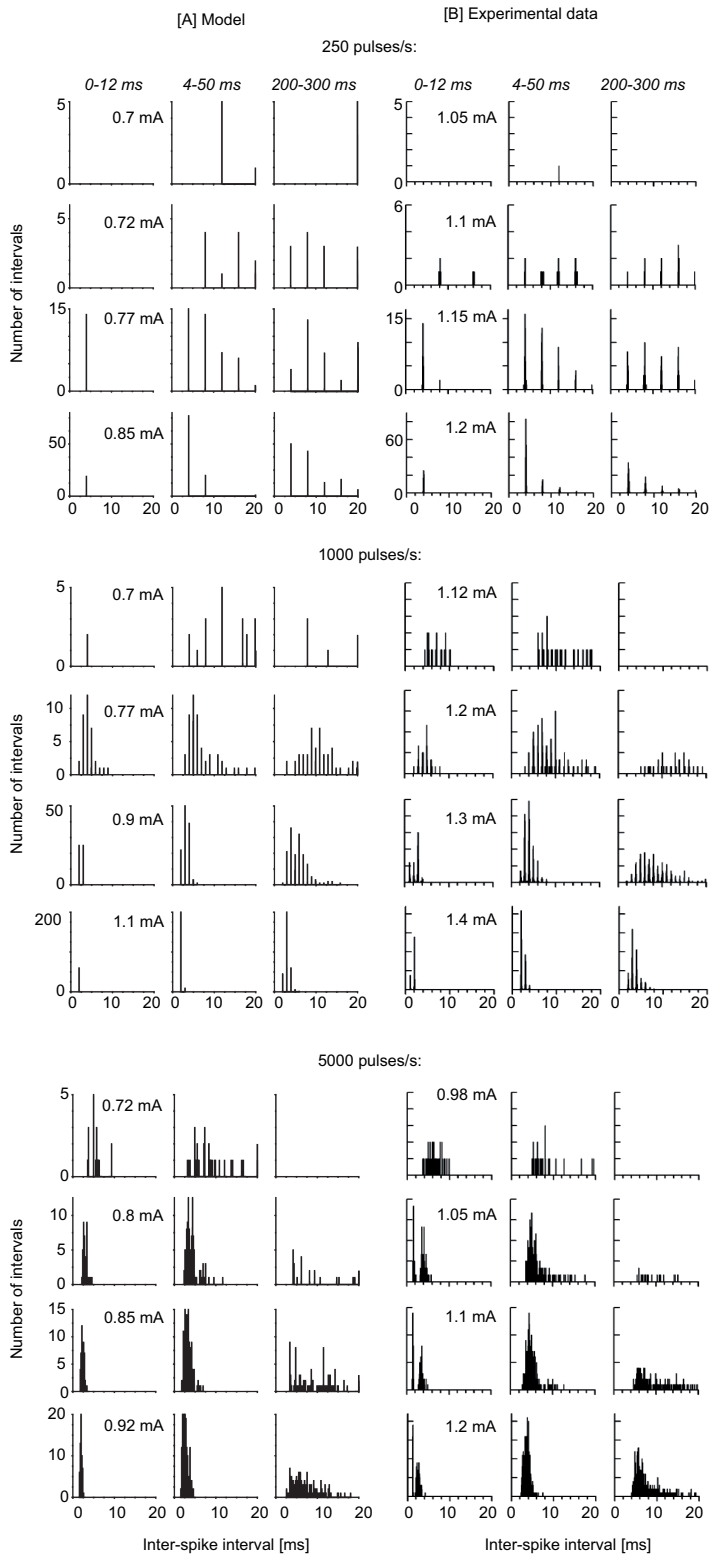
3.3 Interval histograms

The IHs were obtained to replicate the data from Miller et al. (2008) and are shown in figure 2.9. The IHs calculated from modeled responses are shown in the upper four rows, and those from experimental data are shown in the lower four rows. As in the PSTH simulations, for this IH simulation all model parameters were set to the average values (table 2.2). At all rates, the distributions were wider at later epochs; in the 0-12 epoch, especially at higher amplitudes, the intervals were mostly around 5 ms or shorter, whereas intervals of 10-20 ms were detected in both the animal and experimental data in the 200-300 ms epoch. When stimulated with 1000 or 5000 pps, both animal and simulated data exhibited a widening of the IH distribution and lowering of the peak in the last epoch compared to the second epoch. When stimulated with the largest amplitude at a rate of 5000 pps, the peak doubled from 10 to 20 intervals from the first to the second epoch and decreased back to 10 in the last epoch. The peak shifted from approximately 2 ms to 5 ms from the first to the last epoch in both the experimental and simulated data. The double peak at onset observed in the animal data when stimulated with the 5000 pps pulse train was missing in the simulations.

3.4 Spike rate decrements: 1200 and 4800 pps

Spike rate decrement data for a group of fibers was calculated to replicate measurements of multiple fibers by Litvak et al. (2001). Figure 2.10 shows the modeled [A] and the experimental data [B] for the final discharge rate, defined as the discharge rate in the last bin, versus the initial discharge rate (the discharge rate in the first bin). Decrements of fibers stimulated with a pulse rate of 1200 pps are shown as grey diamonds and those stimulated with a pulse rate of 4800 pps are shown as black stars.

Figure 2.9 (opposite). Interval Histograms. Examples of IHs obtained by simulations [A] and animal experiments [B] (Miller et al., 2008) by stimulating a fiber 300 ms with three different pulse rates (groups of columns) and four different amplitudes (rows). Stimulus levels are indicated at the left panel per rate and amplitude. For each different rate and level the IH at three different time windows are obtained, 0-12 ms, 4-50ms and 200-300 ms, labeled at the top in italic. Bin-width was set to 50 μs.

[A] Model

[B] Experimental data

250 pulses/s:

1000 pulses/s:

5000 pulses/s:

Inter-spike interval [ms]

Inter-spike interval [ms]

2

37

When stimulated with 24,000 pps all modeled fibers showed complete adaptation. For the simulations, different fibers were used and their parameters were randomly drawn from the distributions. The results were visualized by plotting the final spike rate (average rate over 140-150 ms after onset) on the ordinate vs. the initial spike rate (in the epoch 10-20 ms after onset) on the abscissa. The two dotted lines in the left graph show the linear fit through the origin and the 1200 pps data (upper line) and 4800 pps modeled data (lower line). As shown by the linear regression lines, the highest stimulus rate (4800 pps) caused a lower final discharge rate than the 1200 pps stimulus rate pulse train. This difference in the decrease in discharge rate was visible in both experiments and simulations. There was a broad distribution of final vs. initial discharge rates in both the animal data and simulations.
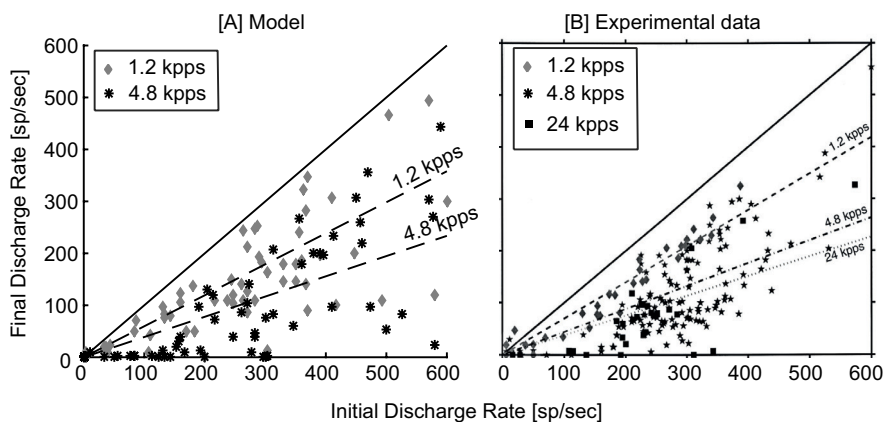

Figure 2.10. Final discharge rates. Modeled [A] and experimental data [B] (Litvak et al., 2001, reprinted with permission) showing the final discharge rate versus the initial discharge rate of different fibers in response to stimulus trains with a pulse rate of 1200 pps (grey diamonds) and 4800 pps (black stars). The 24,000 pps stimulus train was not modeled. For the simulations different fibers were used, their parameters randomly drawn from the distributions. Results are visualized by plotting the final spike rate (average rate over 140-150 ms after onset) on the ordinate vs the initial spike rate (in the epoch 10-20 ms after onset) on the abscissa. The two dotted lines in the left graph show the linear fit through the origin and the 1200 pps data (upper line) and the 4800 pps modeled data (lower line). Each point in the modeled data is based on 30 averages per fiber, 10 different fibers (every 10th fiber from 12000 to 12100) were stimulated at amplitudes of 0.85, 0.86, 0.87 and 0.88 mA.

3.5 Spike rate decrements: 250 to 10,000 pps

Discharge rate decreases were simulated and compared to recordings by Zhang et al. (2007) (figure 2.11). The spike rate decrements are plotted on the ordinate and the onset rate on the abscissa.
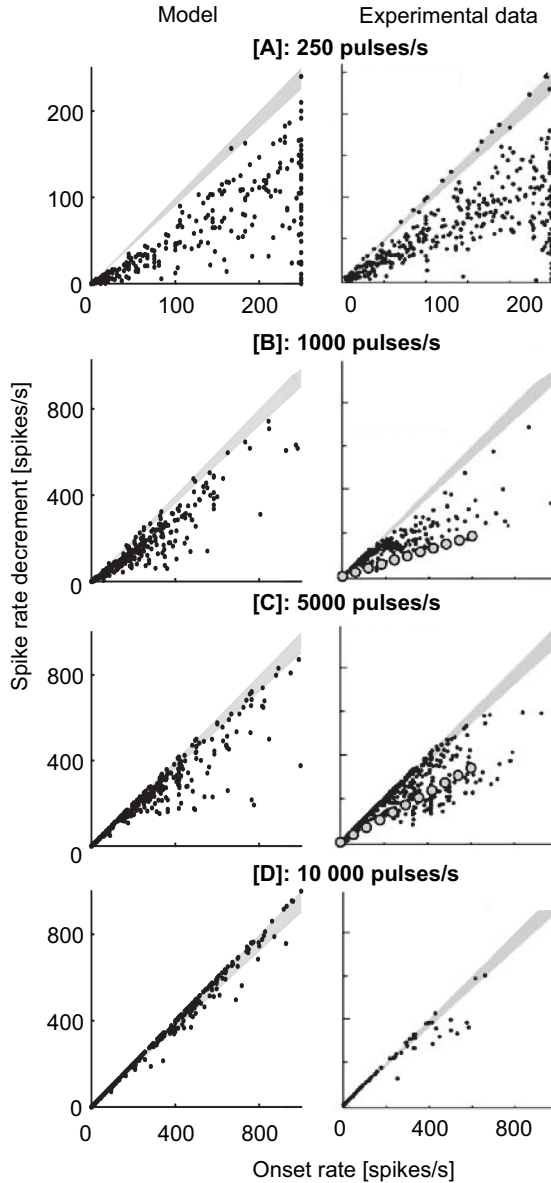
2

Figure 2.11. Discharge rate decreases. Modeled [A] and measured [B] (Zhang et al., 2007, reprinted with permission) rate decrements for 300 ms pulse trains with rates of 250 pps [A], 1000 pps [B], 5000 pps [C] and 10000 pps [D]. Results are visualized by plotting the final spike rate (average rate over 200-300 ms after onset) on the ordinate vs the initial spike rate (in the epoch 0-12 ms after onset) on the abscissa. The gray areas indicate a rate decrement of 90% or more of the initial discharge rate, thus very strong adapters. The gray circles in the animal data plotted at 1000 and 5000 Hz are the aveage rate decrements for the fiber evaluated by Litvak et al (Litvak et al., 2001) at 1200 and 4800 Hz respectively. For the simulations 30 trials were done for forty different fibers (every 10th fiber from 12000 to 12400) of which the parameters were drawn randomly from the normal distributions. Amplitudes used were 0.3 to 0.9 with a step size of 0.02 mA.

With increasing pulse rate there was an increase in adaptation and the spike rate decrements got closer to the initial spike rate. This was seen in both the simulations and the experiments. The average spike rate decrements for pulse trains with a rate of 250 pps were approximately half of the initial discharge rate. At a stimulus rate of 1000 pps, the average discharge rate decrements were higher, especially when the initial discharge rates were low. With a stimulus pulse train of 5000 pps, the rate decrement for trains with an initial discharge rate of up to about 250 pps was equal to the initial discharge rate. With stimulation of 10,000 pps there was almost complete adaptation for nearly all initial discharge rates. At all rates there was a deviation from the mean due to the variability of the model parameters. This variability in rate decrements was similar in the model and the animal experiments.

3.6 Whole nerve simulations

In figure 2.12, both the deterministic single pulse thresholds and the final discharge rates are plotted. In light grey (left y-axis) the average discharge rate per nerve fiber is shown, and the dark lines (right y-axis) indicate the deterministic single pulse thresholds. The discharge rates are averaged over the response to 200 ms stimulation. Every ten neighboring fibers have the same deterministic single pulse thresholds but different stochastic and temporal properties. Fibers with low thresholds had high firing rates and those with high thresholds had low firing rates. There was a large variability in discharge rates at fibers with the same deterministic single pulse thresholds due to their different properties. The deterministic single pulse threshold distribution had a strong effect on the final firing patterns.
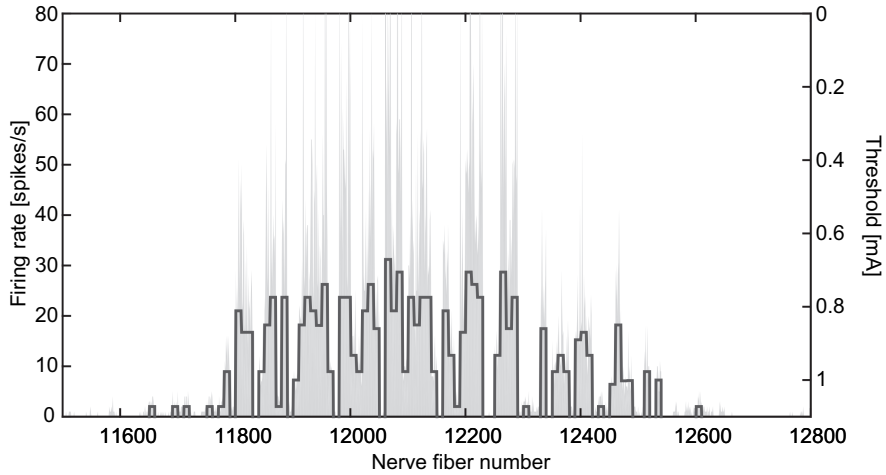
2

Figure 2.12. Whole nerve stimulation. 200 ms stimulation at electrode 8 with a rate of 2000 pps and an amplitude of 0.85 mA. Light gray (left y-axis) shows the average discharge rate per nerve fiber. Some fibers fire with very high pulse rates, up to 200 pps, not shown in this figure. The dark lines (right y-axis) indicate the deterministic singe pulse thresholds as obtained from the 3D active nerve fiber model. Only the stimulated fibers, fiber 11500 to 12800, are shown.

Figure 2.13A shows the spike pattern of the stimulated region of the nerve in response to a pulse train with large stimulation amplitude. Figure 2.13B shows a color-coded plot of the number of spikes in bins of 25 fibers and 7 ms. Figure 2.13C shows the number of spikes in similar bins divided by the number of spikes in the first bin for every fiber. The figure shows that the fibers at the edges of the stimulated region adapted more strongly than the fibers in the center of the stimulated region.
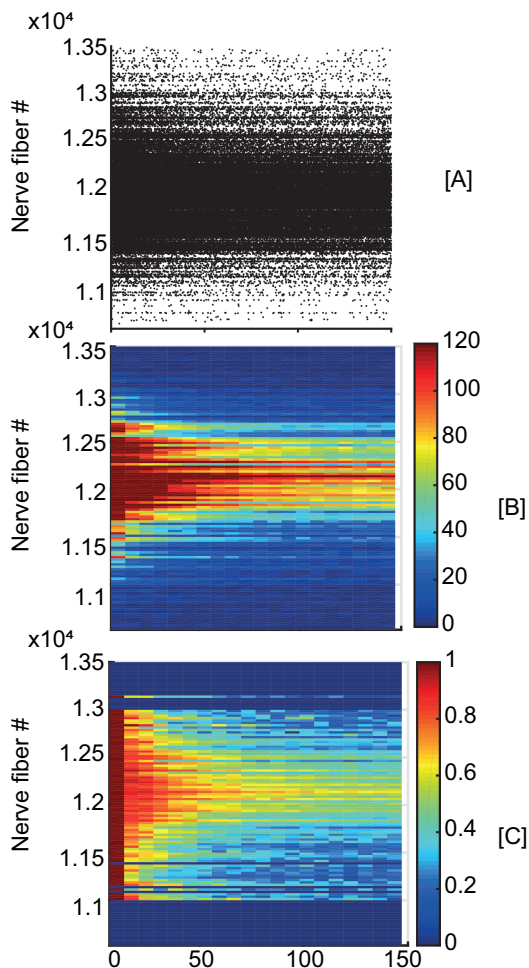
Figure 2.13. Location dependent adaptation. Nerve firing in response to a loud (1.4 mA) 150 ms pulse train with a rate of 5000 pps presented to electrode 8. Nerve fibers shown are 10500 to 13500, the center of nerve fibers stimulated by this pulse train. [A] spike raster plot showing a black dot every time a nerve fiber fires. [B] integrated nerve firing over windows of 25 fibers and 7 ms. Red indicates largest amount of firing per integration window, blue indicates no firing. The colors in the colorbar indicate the number of spikes in each bin. [C] The normalized firing in the integration window. In every window the firing is divided by the numbers of fibers firing in the window immediately after pulse train onset for those 25 fibers. For the normalization only fibers were taken that had more than 15 spikes in the initial bin Where the initial numbers of firings in that bin were larger than 15, the normalized onset firing is equal to 1, here indicated in red. The colors in the colorbar indicate the normalized number of spikes in each bin.

4 Discussion

The model described in this paper is the first to combine a detailed geometric distribution of nerve fibers with stochasticity, refractoriness, adaptation and accommodation. It accurately simulates spike timings in response to long duration pulse trains as observed in a variety of animal experiments. Most models predicting auditory nerve responses to electrical pulse trains are single node models or include a homogeneous spread of the current. The model presented here includes a realistic 3D volume conduction model and thresholds of 32000 nerve fibers calculated with an active nerve cable model. To accurately predict temporal behavior in response to long duration pulse trains the model includes long term temporal parameters. Whilst most temporal models of auditory nerve responses to electrical stimulation include refractoriness, the inclusion of adaptation is less frequently reported (Negm and Bruce, 2008; Woo et al., 2009), and we are the first to publish a model that also includes an accommodation component. The presented model is shown to predict the auditory nerve responses to constant amplitude, long duration, and high-rate pulse trains. The ranges of discharge rate I/O curves, PSTHs, IHs, and rate decrements measured in animal experiments were all very similar to predictions done using the proposed model. Because of the extensiveness of the presented model in as well the spatial as the temporal domain, it can be used to evaluate whole nerve responses to pulse trains. Initial results show remarkable effects of cochlear position on temporal behavior. Because of the efficient implementation of temporal behavior, whole auditory nerve responses to long duration pulse trains, and thus different CI sound coding strategies, can be obtained.

4.1 Model parameters

The exemplary single fiber data could all be replicated by choosing the average model parameters. Replication of these fibers' responses could be improved by searching for a specific parameter set within the distribution of model parameters for the unique fibers. Group data was simulated by randomly choosing fibers from the whole nerve, which yielded similar distributions of fiber responses as seen in animal data. The model is validated by comparison with data obtained from experiments in cats. SFAP measurements are the most suitable measurement to compare predicted spike timings because SFAP is a direct measure of neural activity. A difficulty in the interpretation of SFAP measurements is that the exact measurement position relative to the nerve and stimulating electrode is unknown. As different CIs are used in the animal experiments and some details about the stimulation, such as voltage compliance and distance of the fiber from the electrode, are unknown, the absolute amplitude values are not comparable to the amplitudes used in the simulations. In addition, sometimes only the unexpected recordings of single fibers are presented in papers, making it difficult to derive model parameters for a model of the whole nerve. In the model presented here the distribution of fiber characteristics is assumed to be independent of the location of the nerve fiber along the basilar membrane. However, it is known that the fiber diameter varies with position along the basilar membrane and is related to some of the fiber properties

described by parameters in our model (Liberman and Oliver, 1984; Verveen, 1962). As suggested by Woo et al. (2010), greater rate adaptation may be associated with smaller auditory nerve fiber diameter. This suggestion is based on the observation by Zhang et al. (2007) that strong adapters have higher thresholds. As fibers with larger diameters are mainly located towards the cochlear apex, this could be approximated by implementing a cochlear location-dependent adaptation in the model. Dependency of nerve fiber parameters on cochlear position could be implemented in a further refinement of the model. Other difficulties in the interpretation of animal data arise since averaged data is obtained using a variable, and not always exactly reported, number of trials; Litvak used 20-40 trials per data point (Litvak et al., 2001), and Miller and Zhang used 30 to 100 of trials per point (Miller et al., 2008; Zhang et al., 2007). Due to the complexity of obtaining SFAP measurements, statistical sampling is limited (Woo et al., 2010). The SFAP measurements are all obtained from cat auditory nerve fibers, which are morphologically and physiologically different from human auditory nerve fibers, for instance in diameters and myelination (Liu et al., 2015; Paintal, 1966; Spoendlin and Schrott, 1989). It would be preferable to relate model output to human data, as for instance human ECAPs. Because the model presented in this paper encompasses the whole nerve, ECAP measurements can theoretically be simulated. The pattern of the ECAP depends on the interplay of the spatial distribution and the different temporal and stochastic components in the model. In a follow-up study the model parameters could be optimized for the human auditory nerve by simulating the ECAP in response to pulse trains. The SFAP data in the animal experiments used for the validation was obtained in acutely deafened animals, whereas duration of deafness affects the neural responses (L. F. Heffer et al., 2010; Ramekers et al., 2015). It would be interesting to use the proposed model to simulate full nerve ECAP responses as well as partial nerve ECAP responses to test the theoretical effect of neural degeneration on ECAP measurements.

Stochasticity

Stochasticity is implemented in various parts of the model; by using a stochastic distribution of thresholds over all nerve fibers, a threshold variability, an internal variability of the refractoriness and a distribution of model parameters over the fibers. Figure 2.12 shows that initial thresholds have a strong effect on overall discharge rates in responses to long duration pulse trains. The stochastic distribution of thresholds thus causes a nonhomogeneous distribution of firing rates over nerve fibers in response to continuous pulse trains. As previously shown by Bruce et al. (1999a, 1999b), RS is an essential model parameter to obtain I/O curves similar to animal data in response to electrical pulse trains. Bruce's model predicts smooth I/O curves, whereas animal data show rather rocky increases of discharge rates with stimulus intensity. We hypothesized that this rocky slope is a consequence of internal stochasticity. Our model used a similar approach as Bruce et al, but also implemented internal variations of refractoriness, and as expected produced rocky I/O curves. It is known from the literature that the RS depends on time since the last action potential (Imennov and Rubinstein, 2009; Matsuoka et al., 2001). The effect of such a dependency could be investigated by inclusion in a future version of the model. We

2

expect that this would lead to larger discharge rate variability at higher stimulation rates, and perhaps lead to a lower predicted detection thresholds as was shown by Badenhorst et al. (2015). In neurons there is also a stochasticity in the arrival times of the spikes, referred to as jitter. The proposed model is specified at fiber level and conduction times are neglected. Latencies and jitter can be implemented using a phenomenological approach for a complete fiber, similar to proposed by Hamacher et al., chapter 3.5.3 (Hamacher, 2004). The lowest latencies and jitter occur with the highest stimulation amplitudes. The model could be refined by introducing a stochastic delay (latency with jitter), depending on amplitude of stimulation. Alternatively, jitter in the nodes of Ranvier could be picked up in a future refinement of the biophysical model.

Refractoriness
The effects of refractoriness interplay with the effects of accommodation and adaptation. The effects of refractoriness are mostly visible at short time scales, for instance in onset rates and initial rate decrements. Miller et al. (2008) suggested that the shape of the IHs are determined mostly by refractory properties. Larger refractory parameters in the model lead to larger inter-spike intervals in the IH. Our model shows very similar peak heights and timing in the IHs as the experimental data, supporting that the choice of refractoriness are realistic values. In the interval histograms it was observed that the double peak at onset, which is present in the animal data when stimulated with the 5000 pps pulse train, was missing in the simulations. Zhang et al saw these responses in 27% of the fibers stimulated with these rates and amplitudes. They hypothesize is that it is related to the combined effects of refractoriness and rapid adaptation. Our model does not predict these double peaks, it is thus an unexpected artefact of the model; parameters as included in the proposed model do not explain this variable.

Adaptation and accommodation
The steepness of the slopes in figure 2.5 predicted by the model were more similar to the animal data published by Dynes et al. (1996) than predictions previously modeled by Bruce et al. A difference between this model and the model presented here is the inclusion of adaptation in our model, which results in a shallower slope. The accommodation effect is not prominent in the discharge rate I/O curves in figure 2.5, probably because only low rates, up to 800 Hz were used. The rate decreases in the calculated PSTHs in figure 2.8 were very similar to those obtained in animals by Zhang et al. (2007) for the different rates and amplitudes. These rate decreases occur both initially, mostly due to refractoriness, and at later time scales (up to 100 ms) mostly due to adaptation and accommodation. The accommodation effect is visible in the PSTHs in figure 2.8, where adaptation is stronger with increasing stimulus rate. The PSTHs published by Zhang et al. (2007) were modeled previously by Woo et al. (2010), who also demonstrated an effect of electrode position on rate adaptation. In the simulations the same fiber was used for all four different rates. In the experiments, the fiber stimulated with the highest pulse rate was another fiber. Despite of a larger stimulus amplitude used here, this fiber still shows a stronger adaptation than at lower rates. This can be easily simulated by modeling the fiber stimulated with 10,000

pps off-center of stimulation. The difference between the middle and last epoch in the IHs in figure 2.9 is due to adaptation. The IHs showed rate-dependent adaptation, as the rate decrease from the second to the last epoch was largest when stimulated with the highest rate pulse trains.

The range of spike rate decrements for nerve fibers in response to different rate pulse trains predicted by the model's parameters are similar to ranges of measured decrements as can be seen in figures 2.10 and 2.11. The rate decrement data in figures 2.10 and 2.11 for different fibers exhibited a very similar dependency on pulse rate in the model and in animal experiments. The rate decrements for both pulse rates shown in figure 2.10 were somewhat stronger in our model than in Litvak's data, matching the study published by Miller et al. (2008) in which the group data showed slightly stronger adaptation (figure 2.11). The spread in rate decrements observed by Litvak and Miller et al. was similar to the spread in rate decrements predicted by our model. The spread in decrements in the model is a consequence of the implemented distribution of refractory and adaptation parameters over nerve fibers. The simulations of rate decrements fairly closely matched the animal data up to 10000 Hz. However, at the 24.000 pps stimulation rate our model predicted complete adaptation, which was not observed in animal experiments, as seen in figure 2.10B. Maximal adaptation could be a consequence of saturation of the underlying physiological system, for instance an external Potassium concentration decaying over time (Woo et al., 2009). The animal data show that saturation of the adaptation occurs over time with rates as high as 24 kpps. There would be several options to modify the parameters in order to have the adaptation at 24kpps fit with the physiological data. A simple option would be to include a maximum value for adaptation. However it would also be likely that there is a gradual decrease in the increase of adaptation with rate. We have chosen not to implement a saturation as to our knowledge this is the only experiment available at this rate. To investigate which one is more closely related to the biological situation more data at high rate electrical stimulation is needed.

The time constant in the current model is assumed to be similar for both accommodation and adaptation. However, from a biological perspective it would be reasonable to assume that these different processes decay with different time constants. Accommodation depends mostly on the stimulus itself and could be affected by stimulus shape, but no data has been published yet regarding the effect of stimulus shape on accommodation in auditory nerves. To find the correct dependencies of accommodation parameters on pulse shapes and to validate models, more animal experiments data including longer stimulus durations and a larger variance of stimulus rates and amplitudes are required. In modern neuroscience the origin and relevance of accommodation, sometimes referred to as sub-threshold adaptation or stimulus-specific adaptation, is subject of discussion. A proposed model relates voltage activated K+-current to input-dependent adaptation, whereas calcium activated K+-currents were related to spiking dependent adaptation (Prescott and Sejnowski, 2008). It has been proposed in amodel study by Negm and Bruce that stimulus dependent adaptation is caused by hyperpolarization-activated cation

channels (Negm and Bruce, 2014). Woo et al show that the implementation of a changing external potassium concentration based on K+ activity in a biophysical model leads to rate-adaptation as seen in the animal data (Woo et al., 2009).

Facilitation

The experimental PSTHs in figure 2.8B show an overall increase in discharge rate at 5000 pps relative to lower stimulation rates. There is evidence in the literature that, in chronic deafened animals, this facilitation plays a role when the fiber is stimulated by pulse trains with rates of approximately 2000 Hz and low amplitudes, when it evokes low onset spike probabilities (L. F. Heffer et al., 2010). There is a large spread in the effect, and its exact dependency on pulse train characteristics such as rate and amplitude level is yet to be investigated more thoroughly in animal experiments. Because the effect is seemingly only related to a narrow distribution of pulse rates and amplitudes and is not yet very well understood, we have chosen not to include facilitation in the model, consequently the model's predictions deviate from the animal SFAP data where the effect of facilitation is seen.

Whole nerve simulation

Since the deterministic single pulse threshold distribution has a large effect on final firing patterns, as shown in figure 2.12, it is of importance to include an accurate and realistic 3D volume conduction model. The 3D volume conduction model that we have incorporated includes a cochlear anatomy derived from μCT data and contains a realistic spatial distribution of spiral ganglion cells throughout Rosenthal's canal (Kalkman et al., 2015). The electrical conductivities of the model structures were mainly obtained from literature (Briaire and Frijns, 2000); the conductivity values of temporal bone and the cochlear modiolus were obtained by an optimization process that was based on comparing intracochlear potential recordings from CI subjects to simulated values in subject-specific models (Kalkman et al., 2014). The model has been shown to accurately predict or describe loudness balancing curves in current steering (Frijns et al., 2009; Snel-Bongers et al., 2013) as well as loudness growth curves for different types of multipolar stimulation (Kalkman et al., 2015). This paper demonstrates that spike rate adaptation is dependent on spatial location relative to the current source. Relative rate decreases, and thus the amount of adaptation, is largest at the borders of the stimulated area. Adaptation is expected to be related to phase-locking of amplitude modulated input. Increased adaptation at the borders of the stimulated area could thus lead to stronger perception of pitch at borders of the stimulated region. It was suggested by Laneau et al. (2004) that the center of the activated region are most important for pitch perception. A previous modeling study showed that cochlear location of nerve fibers influences initial activation site on the fiber (Westen et al., 2011). The fibers located in the center of stimulation receive larger stimulus amplitudes, which has an effect on the initial location of firing. To test relative contributions of center and off-center fibers to place and rate-pitch perception the modeled auditory nerve response to amplitude modulated pulse trains should be evaluated in a follow-up study. The temporal behavior of the nerve is co-influenced by

the amplitude of stimulation, and thus by electrode position, as shown in a modeling study by Mino et al. (2004). Nerve morphology will affect the outcome of cochlear implant stimulation and has an important role in the interplay of spatial and temporal effects. To take the effects of the nerve's geometry in account and considering the strong effect of initial thresholds on long term nerve activation it is important to include both realistic spatial and temporal effects in a comprehensive model.

Future directions

Since the model incorporates detailed effects in both the temporal and the spatial domain it can be used to predict auditory nerve responses to CI stimulation. Contemporary cochlear implants use amplitude modulated input to convey important speech information in cochlear implants. Validation for amplitude modulated pulse trains as inputs has also been done and will be presented in a follow-up paper. Another interesting aspect is the neural behavior at much longer time scales, such as minutes. Modelling the adaptation as a power-law gives, as shown for the acoustically stimulated auditory nerve by work of Zilany et al. (Zilany et al., 2009; Zilany and Carney, 2010), a more realistic prediction of the neural behavior after longer durations of stimulation. An interesting future direction is to investigate power-law functions for prediction of auditory neural responses to electrical stimulation. As stated above, the model can be used to predict ECAP responses to pulse trains and compare those to data obtained directly from measurements in human. This output can be related to the stochastic, refractory, and adapting effects included in the model, and their interplay with the auditory nerve's morphology. Because this model is precise in the geometrical definition, and contrarily to most other models includes as well accommodation as adaptation, it is applicable to predict whole nerve responses. Ultimately the model can be used to predict complete neural spiking patterns in response to CI stimulation using different stimulation strategies. The conservation of temporal and spatial information present in the pulse train at the stage of neural activation can be evaluated. Because of the efficient implementation of spatial and temporal components, the model can easily be used to evaluate whole nerve responses to long duration sound segments. This can facilitate comparison of whole nerve responses to many different input signals, such as varying in amplitude, amplitude modulation, pre-processing, and coding strategies.

Inputs as used in perceptual patient testing such as minimal detection and identification tests can be used in the model. Comparison of simulated auditory nerve responses to perceptual data obtained from cochlear implant users will aid in the interpretation of the produced spiking patterns. As a next step an interpretation model of the spiking patterns in relation to the psychophysical perception of CI users will be built. Such an interpretation model could be used to evaluate complete auditory nerve responses to different sound coding strategies.

Conclusion

A model was developed that accurately predicts auditory nerve responses to long duration CI stimulation with a wide range of stimulus rates and amplitudes. The model is very well defined in the spatial domain and is temporally and stochastically extended. The model's responses were in good agreement with animal data for continuous long duration pulse trains. The model accurately predicts discharge rate I/O curves, PSTHs, IHs, spike rate decrements, and their variances for realistically located auditory nerves stimulated with a wide range of amplitudes and rates. The broad implementation of stochastic behavior results in predictions of variances of measures comparable to those seen in animal data. By combining spatial details with long-term temporal components and a broad implementation of stochasticity, a comprehensive model is developed. It is validated for long duration electric stimulation of a wide range of input parameters and that can be used to evaluate auditory nerve responses to cochlear implant sound coding strategies.